Excitonic complexes in InAs/InP nanowire quantum dots

Michał Zieliński*
Institute of Physics, Faculty of Physics, Astronomy and Informatics and Nicolaus Copernicus University, ul. Grudziądzka 5, 87-100 Toruń, Poland

(Received 22 January 2020; revised manuscript received 8 April 2020; accepted 8 April 2020; published 5 May 2020)

InAs quantum dots embedded in InP nanowires form an important platform for basic research studies, as well as for quantum dot applications. Notably, understanding of nanowire quantum dot spectral properties is essential in both cases. Therefore, in this work we use atomistic theory to study spectra of the single exciton (X), the biexciton (XX), the triexciton (XXX), and the positively and negatively charged trions (X^+ and X^-) confined in these nanostructures. We focus on the role of vertical and lateral confinement, therefore, we systematically study a large family of quantum dots with different heights and diameters, and find the important role of correlations due to presence of higher states. We find that the order of excitonic binding energies is a characteristic feature of InAs/InP nanowire quantum dots being (ordered from negative to positive values): X^-, XX, and X^+, with strongly bound X^-, rather weakly bound XX, and typically unbound X^+. Next, we determine the key role of alloy randomness due to intermixing, which turns out to especially important for larger quantum dot heights and phosphorous contents over 40%. In selected cases, the alloying can lead to an unbound biexciton, and can even reverse ordering of excitonic lines.

DOI: 10.1103/PhysRevB.101.195302

I. INTRODUCTION

Nanowire quantum dots [1,2], grown by the vapor-liquid-solid (VLS) procedure [3,4], offer the advantage of efficient spatial positioning [5–8], with possibility of post-growth tuning [6,7,9], combined with high-quality optical spectra [9–12]. Nanowire quantum dots are often grown on [111] oriented substrates, what by virtue of symmetry should [13–19] lead to highly reduced bright exciton splitting [20,21]. These specific features allow for potential applications of nanowire quantum dots in quantum information and cryptography [22–28].

Apart from the possible control of their position, nanowire quantum dots offer the opportunity of efficient tailoring of quantum dot dimensions via the manipulation of catalyst size [5,10]. Such control, and understanding of physical properties of nanowire quantum dots with respect to their spatial dimension, is in principle essential for further future applications. Therefore, in the following we study spectral properties of [111] oriented InAs/InP nanowire quantum dots that vary by height and diameter, aiming to understand how different quantum dot spatial dimensions and chemical compositions affect properties of various excitonic species confined in these dots, namely, the single exciton (X), the biexciton (XX), and positively (X^+) and negatively charged (X^-) excitons, as well as the complex of three excitons, i.e., the triexciton (XXX).

II. METHODS

We study here selected spectral properties of several excitonic complexes (X, XX, XXX, X^+, and X^-) for a family of disk-shaped InAs quantum dots embedded in InP host nanowire. These quantum dots have heights varying from approximately 1 to 7.25 nm (3 to 18 monolayers), and diameters varying from 20 to 30 nm (Fig. 1), thus covering a broad range of dimensions including those obtained experimentally [5], with diameter-to-height aspect ratios changing considerably from 4 to 30.[1] We consider 10 different heights and 5 different diameters leading to overall 50 various quantum dot systems. More computationally challenging calculations were additionally performed for a family of alloyed nanowire $InAs_{1-x}P_x$ quantum dot, as will be discussed later in the text. The disk shape of quantum dots is expected due to the VLS growth mode and the cylindrical shape of host nanowire. The InP nanowire in which dots are embedded has a diameter equal to 72 nm, thus much larger than quantum dot diameters, corresponding to a case of so-called clad [10] nanowire quantum dots.

The first stage of the calculation starts with finding atomic positions that minimize total elastic energy. This is achieved by using the valence force field method of Keating [29,30] and minimization of strain energy performed with the conjugate gradient method [31]. In the [111] (growth) direction we account for a 120-nm-long section of a nanowire that contains over 18 million atoms. This is sufficient for converged single-particle and many-body spectra [32] of nanowire quantum dot with respect to the host nanowire section length. The valence force method is described in more detail in Refs. [33,34] and in our previous papers [31,35–37]. Next, from atomic positions, the piezoelectric potential [38–42] is calculated by

*mzielin@fizyka.umk.pl

[1]Higher aspect ratio nanowire quantum dots were studied by us in Ref. [16] in the context of heavy- to light-hole exciton transition.

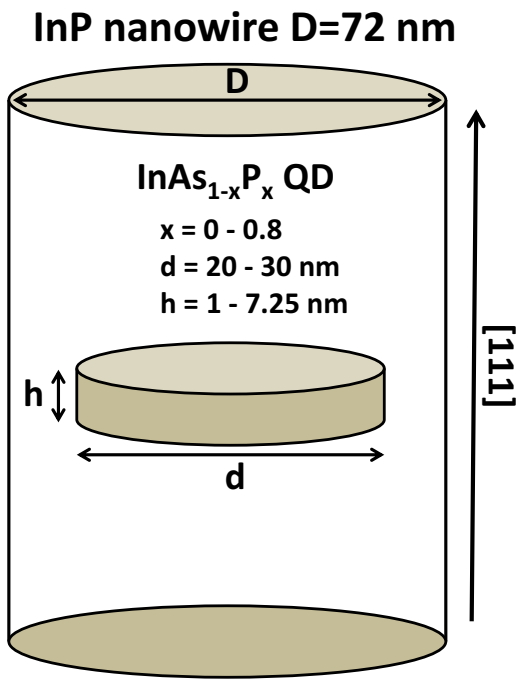

FIG. 1. Schematic view of the system under study: $InAs_{1-x}P_x$ quantum dot embedded in InP nanowire. Nonalloyed InAs quantum dots correspond to $x = 0$. Dimensions are not to scale. See text for details.

accounting for both linear and quadratic contributions. Here, we use piezoelectric coefficients from Ref. [40]. For comparison, and to study the role of piezoelectricity, we also present results calculated with piezoelectric potential artificially neglected. Then, the single-particle spectra of electrons and holes are obtained with the empirical tight-binding method accounting for d orbitals and spin-orbit interaction [36,37]. The single-particle tight-binding Hamiltonian for the system of N atoms and m orbitals per atom can be written in the language of the second quantization as follows [35]:

$$\hat{H}_{\mathrm{TB}} = \sum_{i=1}^{N}\sum_{\alpha=1}^{m} E_{i\alpha} c_{i\alpha}^{+} c_{i\alpha} + \sum_{i=1}^{N}\sum_{\alpha=1,\beta=1}^{m} \lambda_{i\alpha,\beta} c_{i\alpha}^{+} c_{i\beta} + \sum_{\langle i,j\rangle}\sum_{\alpha,\beta=1}^{m} t_{i\alpha,j\beta} c_{i\alpha}^{+} c_{j\beta}, \quad (1)$$

where $c_{i\alpha}^{+}$ ($c_{i\alpha}$) is the creation (annihilation) operator of a carrier on the (spin) orbital α localized on the site i, $E_{i\alpha}$ is the corresponding onsite (diagonal) energy, and $t_{i\alpha,j\beta}$ describes the hopping (off site and off diagonal) of the particle between the orbitals on the four nearest-neighboring sites. i iterates over all atoms, whereas $\langle i, j\rangle$ denotes all pairs of nearest neighbors. α is a composite (spin and orbital) index of the onsite orbital, whereas β is a composite index of the neighboring atom orbital. Coupling to further neighbors is thus neglected, and $\lambda_{i\alpha,\beta}$ (onsite and off diagonal) accounts for the spin-orbit interaction following the description given by Chadi [43], which includes the contributions from atomic p orbitals. Here, we use the $sp^3d^5s^*$ parametrization of Jancu [44]. The tight-binding calculation is effectively performed on a smaller domain than the valence force field calculation [32,45]. However, the number of atoms in the tight-binding computational box still exceeds 0.5 million, and the dimensions of the tight-binding Hamiltonian exceed 10^7. The details of the $sp^3d^5s^\star$ tight-binding calculation were discussed thoroughly in our earlier papers [31,35–37].

Finally, the excitonic spectra are calculated with the configuration interaction method. The Hamiltonian for the interacting electrons and holes can be written in second quantization as follows [46]:

$$\hat{H}_{ex} = \sum_i E_i^e c_i^\dagger c_i + \sum_i E_i^h h_i^\dagger h_i + \frac{1}{2}\sum_{ijkl} V_{ijkl}^{ee} c_i^\dagger c_j^\dagger c_k c_l + \frac{1}{2}\sum_{ijkl} V_{ijkl}^{hh} h_i^\dagger h_j^\dagger h_k h_l - \sum_{ijkl} V_{ijkl}^{eh,\mathrm{dir}} c_i^\dagger h_j^\dagger h_k c_l + \sum_{ijkl} V_{ijkl}^{eh,\mathrm{exchg}} c_i^\dagger h_j^\dagger c_k h_l, \quad (2)$$

where E_i^e and E_i^h are the single-particle electron and hole energies obtained at the single-particle stage of calculations, respectively, and V_{ijkl} are Coulomb matrix elements (Coulomb direct and exchange integrals) calculated according to the procedure given in Ref. [35]. In this approach, not being able to calculate the effective Coulomb interaction self-consistently [47] one assumes a statically screened Coulomb interaction [35,48]. Further, since in this work we study the much larger nanowire diameter than diameters of quantum dots, corresponding to so-called clad [10] nanowire quantum dots, the large dielectric mismatch between the nanowires and their surroundings should not play a significant role [49]. Moreover, the role of image charges at the InAs quantum dot–InP nanowire dielectric interface is expected to be small [50] in part because of much smaller dielectric mismatch [51–53], and in part due to cancellation between the self-energy interaction of each particle with its own image charges and the excitonic corrections [54]. Having said all the above, the role of dielectric interfaces on the spectra of nanowire quantum dots is an intriguing line of research, and will be continued in our future work.

More details on Coulomb matrix element computation for tight-binding wave functions can also be found in Refs. [55,56] as well as in our recent work [57,58].

III. EXCITON

Excitons are formed by interacting electron-hole pairs, it is thus instructive to study first electron and hole single-particle spectra. Therefore, Fig. 2 shows several lowest electron states as a function of nanowire quantum dot height, and for three different quantum dot diameters. As excepted, for disk-shaped quantum dots, electron states form well-defined shell structure [46,59] that remains present for various heights and diameters. For all considered cases, we observe a monotonic decrease of electron energy levels with increasing height (and diameter), as anticipated due to decreased quantum confinement. Thus, there is a pronounced, over 200 meV, ground electron state energy difference between quantum dots of smallest and largest considered heights. Interestingly, with an increasing height, spacings between subsequent shells (e.g., energy

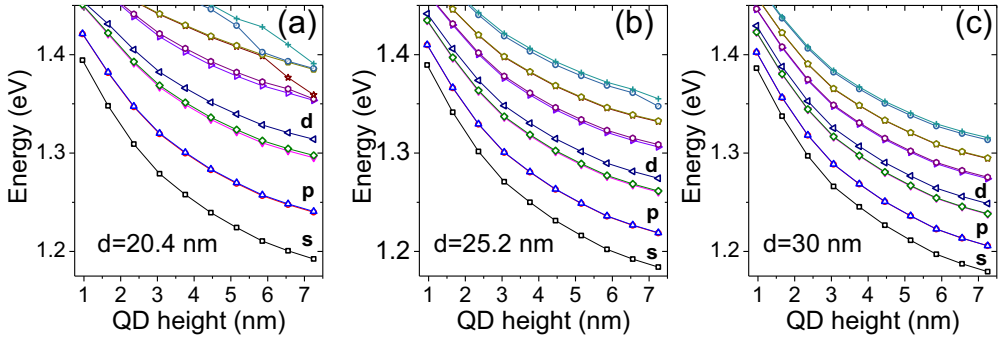

FIG. 2. Dependence of several lowest single-particle electron levels calculated as function of quantum dot height for three nanowire quantum dots of different diameters: (a) $d = 20.4$ nm, (b) $d = 25.2$ nm, (c) $d = 30$ nm. Higher-energy levels are omitted for clarity. Lines connect and order states energetically. Letters mark approximate symmetry of subsequent shells.

difference between s and p levels) increase with height, yet they decrease with diameter. This will have an impact on excitonic complexes' spectra as discussed later in the text. However, electron states demonstrate behavior consistent with predictions of simple models [46], and are presented here mostly for completeness.

Contrarily, hole states, as shown in Fig. 3, reveal non-monotonic change with quantum dot height [16] and generally lack of simple shell structure for quantum dots of larger heights. This is particularly well visible for quantum dots of smaller diameters [Fig. 3(a)] where the hole p shell stands out from the rest of the spectrum for heights up to approximately 3 nm, before crossing with higher excited states. For larger dot diameters, the hole p shell is present until approximately 4.5 and 5 nm heights for diameters 25.2 and 30 nm, respectively. However, for quantum dot heights larger than 6 nm, none of the quantum dots considered here have a well-defined shell structure of hole states. In other words, for "flat" quantum dots the hole shell structure is present for all considered diameters, whereas for "tall", high-aspect ratio quantum dots is it practically not present at all (see also the Appendix). This will play an important role for excited excitonic states, and have an impact on spectra of excitonic complexes as discussed in the following.

Next, Fig. 4 shows the evolution of excitonic ground state as a function of height and diameter. The height of quantum dot goes on the x axis, whereas quantum dot diameter is denoted by diameter (and color/shade) of each data point. This allows to put both height and diameter dependence on a single two-dimensional plot in a form of a "bubble chart" (not to confuse with a contour plot). As shown in Fig. 4, excitonic ground-state energy decreases with respect to both increasing quantum dot height and diameter. The dependence on height is more pronounced due to dominant confinement in the growth direction. However, larger height quantum dots have also bigger spread of energies due to diameter variation. In the considered range of quantum dot sizes, the ground-state excitonic energy changes from about 1000 to 720 meV. This energy shift is mostly attributed to changes in single-particle electron energy due to decreasing confinement with increasing quantum dot height, which was discussed above, and to a much lesser degree to changes of hole single-particle energies, and electron-hole interactions.

For nonalloyed nanowire quantum dots considered here, the exciton has no fine structure of either dark and bright excitons due to strict C_{3v} symmetry [13,15]. Fine-structure splitting due to alloying, and resulting exchange effects, has been studied thoroughly in our recent paper [18]. Additionally, let us note that (isotropic) exchange splitting (also studied in Ref. [18]) between dark (ground and first excited, doubly degenerate) and bright (third and fourth excited, doubly degenerate) exciton states is on the order of hundred μeVs, thus much smaller than energy scale considered in Fig. 4.

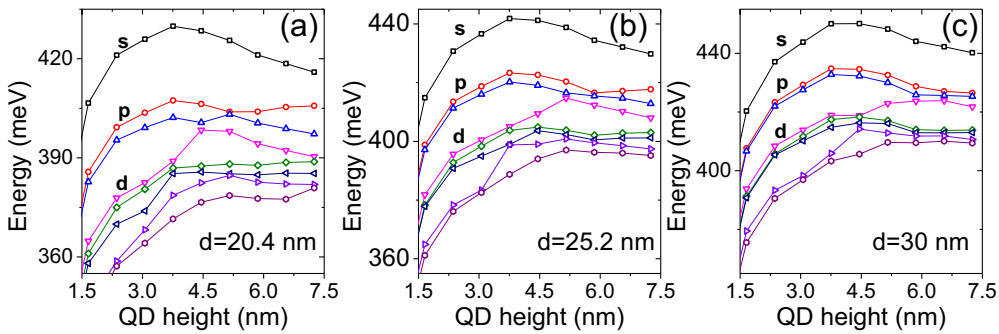

FIG. 3. Dependence of several lowest single-particle holes levels calculated as function of quantum dot height for three [(a)–(c)] nanowire quantum dots of different diameters: (a) $d = 20.4$ nm, (b) $d = 25.2$ nm, (c) $d = 30$ nm. Note reverse ordering of hole levels and different energy scales on each plot. Higher-energy levels are omitted for clarity. Lines connect and order states energetically. For clarity, only spectra of quantum dots with heights larger than 1.6 nm are shown here.

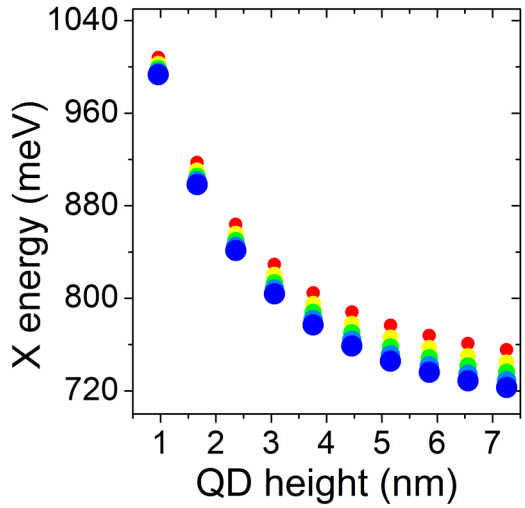

FIG. 4. Evolution of the ground-state exciton energy as function of nanowire quantum dot height and diameter. There are results for 10 different heights and 5 distinct diameters shown here. Quantum dot diameters correspond to size/color of each circle on the plot.

The single exciton is a fundamental object studied in nanowire quantum dots, and the energy corresponding to emission from its bright states acts as a reference level to all other complexes studied in the following.

IV. NEGATIVELY CHARGED EXCITON

Exciton with an additional electron forms a negatively charged exciton X^-, also know as a negative trion [46,59,60]. In the photoluminescence experiment (that could be viewed as electron-hole pair recombination in a presence of an additional electron) one does not measure the trion's ground-state energy, but rather emission energy defined with respect to a neutral (single) exciton. Therefore, Fig. 5(a) shows quantum dot size dependence of negatively charged exciton binding energy, defined as an energy difference between charged and neutral excitons' optical emission line energies. Negative values of binding energies correspond to the charged exciton emission energy lower than the neutral exciton. In such situation, the charged exciton is considered to be bound with respect to the neutral one. Figure 5(a) shows that the absolute value of X^- binding energy generally decreases with the increasing quantum dot height and diameter. For smaller quantum dot heights, the X^- binding energy is on the order of -4 meV, whereas for largest height dots it reaches approximately -2 meV. Notably, the X^- binding energy depends rather strongly on the diameter for small height quantum dots. One could argue that for low-height quantum dots, the overall confinement is effectively more strongly reduced by the increase of the diameter than for higher quantum dots which already have much lower confinement in the growth direction. One can quantify this statement by using a formula to describe negatively charged excitons binding energy as [19,61–63]

$$E_{X^-} = J_{ee} - J_{eh} + \mathrm{corr}(X^-), \tag{3}$$

where J_{ee} is the electron-electron repulsion, J_{eh} is the electron-hole attraction (hence minus sign), both calculated for electron and hole in their ground states, corr is a correction due to the presence of higher levels, i.e., configuration mixing, as well as exchange interaction due to spin degrees of freedom [20]. However, since the exchange term is relatively small (fraction of a meV), and the magnitude of corr is typically dominated by mixing of configuration, from now on, we will call corr shortly as related to correlations. Let us also note that ground excitonic states of all complexes studied in this paper are dominated by configurations (with different spin alignments [46]) involving predominantly ground electron and hole states (both doubly degenerate due to spin [20]). These ground-state contributions are usually well over 90%, however, despite being much smaller, contributions due to higher states still play significant role in excitonic spectra, as shown further in the text.

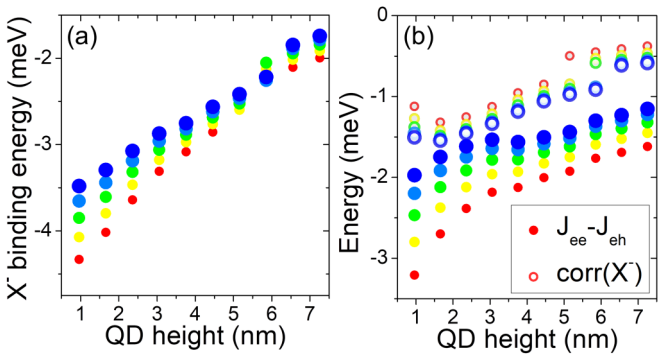

FIG. 5. Negatively charged exciton X^- binding energy (a), and its division (see the text) into contributing components (b) as function of nanowire quantum dot and diameter. Quantum dot diameters correspond to size/color of each circle on the plot.

Equation (3) allows therefore to decompose the E_{X^-} binding energy into a "Coulomb direct" term $J_{ee} - J_{eh}$ and a term due to correlations corr(X^-) as shown on Fig. 5(b). Additionally, individual J_{ee}, J_{eh}, and J_{hh} integrals size dependencies are shown in the Appendix for comparison. Figure 5(b) shows that the Coulomb direct term (full circles) is mostly responsible for the overall dependence of E_{X^-} binding energy with height, with strong height dependence of its magnitude. Notably, the value of E_{X^-} is negative, with both contributing terms [$J_{ee} - J_{eh}$ and corr(X^-)] being of the same sign. Binding energy of X^- is mostly related to negative value of $J_{ee} - J_{eh}$, and thus larger magnitude of J_{eh} than J_{ee}, indicating stronger electron-hole attraction (see the Appendix) that electron-electron repulsion, and therefore stronger spatial localization of hole states than electron states. In the language of continuous matter approximation, this difference between electron and hole integrals could be traced back to larger effective mass of hole states, and the fact that particles with larger mass tend to localize more in a given potential [64]. This can be assessed in terms of numbers. For example, for a family of quantum dots of 3 nm height the electron has approximately 57% of its charge density localized in the quantum dot region with pronounced 43% tails in the nanowire. For the same height, the ground hole state has over 97% of its charge density in the quantum dot volume. However, for $h = 7.2$ nm the ground electron state is 88% confined in the quantum dot, and the

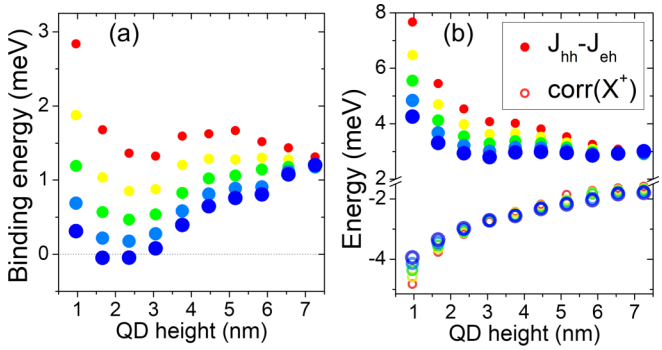

FIG. 6. Positively charged exciton X^+ binding energy (a), and its division (see the text) into contributing components (b) as function of nanowire quantum dot and diameter. Quantum dot diameters correspond to size/color of each circle on the plot.

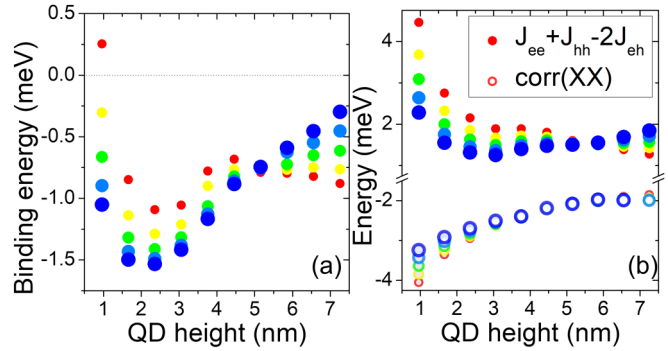

FIG. 7. Biexciton XX binding energy (a), and its division (see the text) into contributing components (b) as function of nanowire quantum dot and diameter. Quantum dot diameters correspond to size/color of each circle on the plot.

hole state has over 99% of its charge in the dot area. In the latter case $J_{ee} - J_{eh}$ difference should be smaller and hence contribute less to X^- binding energy. Moreover, the increase of quantum dot dimensions, and the larger volume for the electron and the hole to occupy, leads to smaller Coulomb interactions, as is manifested in typically decreasing values of all J integrals with quantum dot sizes (see the Appendix).

The corr(X^-) correction due to correlations [empty circles on Fig. 5(b)] varies between -1 and -1.5 meV for low-height quantum dots, and is approximately equal to -0.5 meV for largest considered heights. The corr(X^-) is negative as correlations are generally expected to reduce excitonic complexes' energies [46,60]. For quantum dot heights of 5 and 6 nm there is an apparent gap in corr(X^-) value, which is related to a complicated level structure of excited hole states at these quantum dot heights [since corr(X^-) accounts for higher shells], and it transforms to a visible, yet weak, reversal of X^- binding energy trend with diameter for $h = 6$ nm [Fig. 5(a)]. Generally, however (as constituted by two electrons and only one hole), X^- complex is rather weakly affected by peculiarities of excited hole states.

To summarize, the negatively charged exciton binding energy is determined mostly by properties of electron and hole in their ground states, with a relatively small correction due to excited states. The magnitude of X^- binding energy generally decreases with height and diameter, showing a larger spread of values with respect to the diameter for flat dots, and a small dependence on the diameter for taller dots.

V. POSITIVELY CHARGED EXCITON

Consistently, an exciton with an additional hole forms a positively charged exciton X^+, also known as a positive trion [46,59,60]. Analogously, its binding energy can be given as [19,61–63]

$$E_{X^+} = J_{hh} - J_{eh} + \mathrm{corr}(X^+), \tag{4}$$

where J_{hh} is the hole-hole repulsion, consistently calculated in the ground hole and, respectively, corr(X^+) is a correction to E_{X^-} due to presence of higher levels (correlations and exchange interaction). Figure 6(a) shows positively charged exciton binding energy as a function of quantum dot height and diameter. This energy is typically positive, yet the height dependence is nontrivial, varying from about 0 to 3 meV for smallest quantum dot heights, and showing very little diameter dependence for highest considered quantum dots (with values close to 1.25 meV). Only for two considered heights (close to about 2 nm) and largest considered diameters, the binding energy has small negative values. Moreover, the height dependence is nonmonotonic and the binding energy decreases with height up to approximately 3 nm, and then the trend is reversed.

The distribution of excitonic values with diameter is related to the spread of $J_{hh} - J_{eh}$ values as shown in Fig. 6(b). This can vary from 3 up to even 8 meV, and origins from different degrees of the electron and hole spatial localization, analogously to a previously discussed case of X^-. Interestingly, $J_{hh} - J_{eh}$ has a positive sign (since the hole is generally more confined), whereas corr(X^+) maintains a negative sign. This latter correction has, however, larger magnitude than for X^-, and varies from approximately -4 to -2 meV. Arguably, correction due to correlations is more pronounced for E_{X^+} due to smaller level spacing of hole states as compared to electron states, and thus stronger configuration mixing.

In summary, positively charged exciton X^+ is generally unbound (i.e., has emission energy larger than X) and shows substantial diameter dependence for small quantum dot heights, and contrarily very little diameter dependence for larger quantum dot heights.

VI. BIEXCITON

Recombination of an interacting electron hole in a presence of another electron-hole pair leads to a biexciton emission spectra. Similarly to charged complexes, the biexciton binding energy can be written as [19,61–63]

$$E_{XX} = J_{ee} + J_{hh} - 2J_{eh} + \mathrm{corr}(XX), \tag{5}$$

with all the notations consistent with previously analyzed cases. The XX binding energy is typically weakly negative (with the exception of one, smallest considered quantum dot) and revealing a complicated size dependence as shown in Fig. 7. This complexity is related to a nontrivial size dependence of $J_{ee} + J_{hh} - 2J_{eh}$ as shown in Fig. 5(b). Here, the

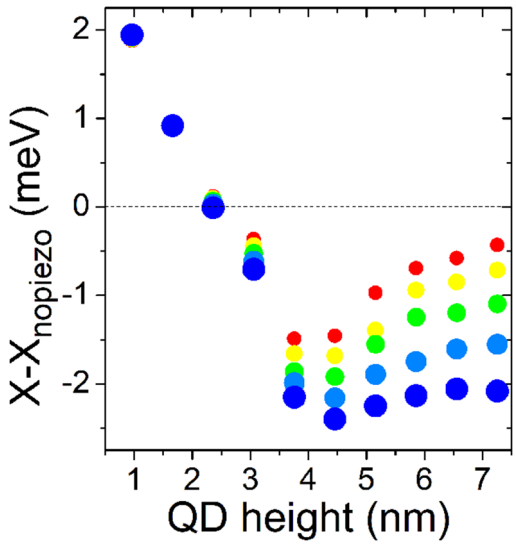

FIG. 8. Excitonic ground-state energy difference between cases with and without piezoelectricity accounted for (see text for details). Quantum dot diameters correspond to size/color of each circle on the plot.

$J_{ee} + J_{hh} - 2J_{eh}$ term can be viewed as sort of measure of a difference between electron-hole attraction and an "average" of electron-electron and hole-hole repulsive interactions. Apparently, this term reverses its diameter dependence, when going from small to large heights, and notably for $h = 5$ nm there is virtually no dependence on the quantum dot diameter. Moreover, corr(XX) is negative with values similar to corr(X^+) leading to an overall negative, though of relatively small magnitude, binding energy of the biexciton.

In summary, in studied nanowire quantum dots, the biexciton is typically weakly bound and shows nonmonotonic trend with respect to both quantum dot height and diameter.

VII. PIEZOELECTRICITY

To further inspect excitonic binding energy size dependencies, in this section we will compare results presented so far with those obtained by artificially neglecting piezoelectricity. We have checked that, for a considered family of nanostructures, piezoelectricity (due to "flat" nanowire quantum dot shape and relatively low strain in InAs/InP nanostructures) has a little impact on absolute single-particle electron and hole energies despite [111] orientation traditionally connected to substantial role of piezoelectricity [65]. Consistently, piezoelectricity has also a little effect on the energy of the ground exciton states. These differences being on a meV scale, and thus so small that they would not be notable either on single particle or on excitonic energy plots showed earlier. However, binding energies of excitonic complexes are related to energy differences, and therefore it is instructive to study piezoelectricity impact on the ground excitonic state energy, as shown in Fig. 8. Here, we present energy difference of excitonic ground-state difference between cases with or without the piezoelectric contribution accounted for. Notably, as mentioned above, piezoelectricity induces rather small, on the order of meVs, shift to single

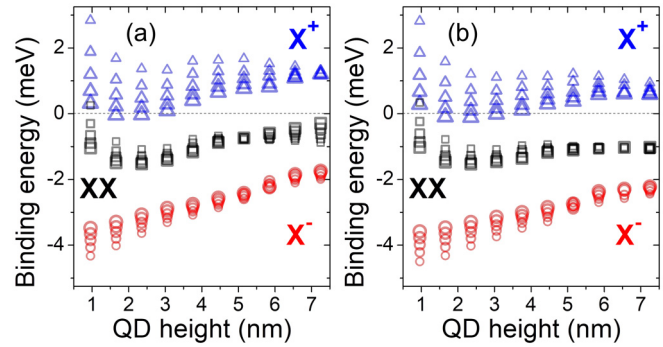

FIG. 9. Comparison of excitonic complexes' binding energies (see text for details) for a case with (a) piezoelectricity accounted for and (b) artificially neglected. Symbols/colors denote different complexes. Sizes of symbols mark distinct quantum dot diameters. See text for details.

exciton ground-state energy. Interestingly, the ground exciton state is shifted to higher energies for low-height quantum dots, and to lower energies for larger-height nanostructures. Moreover, the piezoelectricity induced energy shift depends on the diameter only for high-aspect ratio quantum dots, and shows virtually zero-diameter dependence for flat, low-height nanostructures. Therefore, piezoelectricity may play a certain role only for quantum dots with larger heights, consistent with the usual [66] understanding of piezoelectric potential built up with quantum dot size. Importantly, these energy shifts are related to electron and hole single-particle energy changes due to piezoelectricity, whereas electron-hole interactions are affected by piezoelectric potential on a much smaller sub-meV scale (0.2 meV and less, and as such are not discussed here).

Since the biexciton has the ground-state energy approximately being equal to twice the energy of the exciton, the biexciton ground-state piezoelectricity dependence is qualitatively similar to that of a single exciton, yet multiplied by factor 2, as confirmed by our calculations. The piezoelectricity correction, on a scale of meVs, at first may not appear to be a major contribution to the biexciton spectra, since the biexciton ground-state energy is approximately 2 eV.[2] However, the biexciton emission spectra, as already mentioned, is related to the energy difference of the initial biexcitonic state, and the final single exciton state. In effect, a small correction of excitonic spectra due to piezoelectricity, as shown in Fig. 8, will directly transfer to the biexciton binding energy.[3]

Figure 9(a) therefore shows combined results of X^-, X^+, and XX binding energies with piezoelectricity accounted

[2]The biexciton ground-state energy is approximately twice that of exciton ground-state energy since there are two excitons forming the biexciton state, thus being on a scale of 1–2 eV. This biexciton ground-state energy is, however, not directly measured, but rather the energy difference between the biexciton and the single exciton state [35] is accessible experimentally, and corresponding to biexcitonic line in the quantum dot emission spectra.

[3]We emphasize again that the biexciton recombination is process of electron-hole recombination in a presence of another electron-hole pair, thus leaving the exciton as a final state.

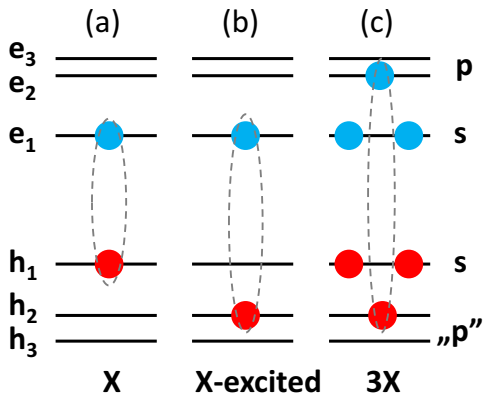

FIG. 10. Schematics of excitonic levels and recombinations involving (a) excitonic *s* shell, (b) excited excitonic states with hole occupying "*p*" shell, (c) triexciton spectra with both electron and hole occupying excited, *p*-shell states.

for, but placed together on one plot. Results obtained by neglecting piezoelectricity are shown in Fig. 9(b). On both figures, for clarity, points corresponding to different diameters are plotted using the same colors (shades), whereas different colors (shades) as well as symbols are now used to mark distinct excitonic complexes. Piezoelectricity generally affects excitonic binding energies rather weakly, and most importantly will not affect the ordering of excitonic lines. The only substantial effect of piezoelectricity can be observed for larger height nanowire quantum dots, where the piezoelectricity is responsible for the change (reversal) of the biexciton binding energy dependence on the diameter.

VIII. *s-p* SHELL SPLITTING

Excitonic complexes studied so far are dominated by configurations involving electrons and holes in their ground states of (approximately) *s* symmetry. To inspect the role of the higher levels, namely the "*p*" shell, one can study higher-lying exciton states involving configurations with electron in the ground state, whereas the hole is placed into excited (*p*-shell) states [shown schematically on Fig. 10(b)]. Figure 11(a) shows therefore the energy difference between the first excited exciton state and the exciton ground state, the former involving the hole h_2 state (using a notation that neglects spin). For quantum dot heights up to approximately $h < 5$ nm, this *s-p* energy difference decreases with quantum dot diameter due to reduced lateral confinement and thus smaller interlevel spacings. Interestingly, the dependence on vertical confinement is quite opposite since as discussed earlier in this paper, the *s-p* single-particle hole spacing first increases with height, yet then (for larger heights) the order of hole *p* states is reversed and the notion of *p* shell is no longer valid. These changes in the single-particle hole spectra for quantum dot height $h > 5$ nm are thus reflected in excited state *s-p* splitting, and its reversal, as shown on Fig. 11(a).

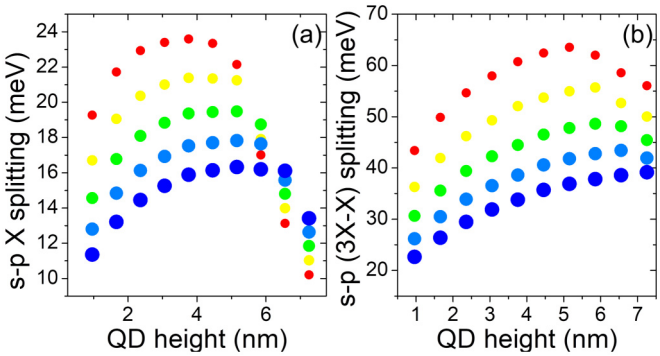

FIG. 11. *s-p* shell splitting calculated for a single exciton (a) and a triexciton (b) as function of nanowire quantum dot and diameter (see text for details). Quantum dot diameters correspond to size/color of each circle on the plot.

However, in a usual photoluminescence experiment one does not observe *s-p* shell splitting by means of excited single-exciton spectra, but rather by increasing laser pumping power to populate quantum dot simultaneously with three excitons forming a triexciton state ($3X$) [46,59]. As shown schematically on Fig. 10(c), the triexciton emission spectra involve (apart from *s-s* recombination) electron and hole recombination from both charge carriers occupying their *p*-shell levels. Since now both electron and hole are in their excited state, the triexciton *s-p* splitting is larger than single-exciton *s-p* splitting. This is shown in Fig. 11(b) with values of this splitting[4] varying from approximately 20 to 60 meV, decreasing with the diameter, thus in good qualitative and quantitative agreement with experimental results [5]. For the triexciton, the magnitude of *s-p* splitting is dominated, and thus determined by the single-particle electron *s-p* shell splitting as studied earlier (Fig. 2). Therefore, similarly to *s-p* single-exciton splitting, it systematically decreases with a diameter, and increases with height reflecting changes of *s-p* electron (e_1 and e_2) level spacings, as shown discussed earlier in the text.

Since the triexciton *p*-shell spectra are dominated by the electron contribution, the lack of shell structure for hole levels does not seem to play a big role for the $3X$ complex, however, for smaller diameter quantum dots one does observe reversal of the *s-p* splitting trend with height. Namely, for small quantum dot diameters *s-p* splitting grows with the height up to about 5 nm and then decreases. Notably, this effect is not present for larger diameter quantum dots.

IX. ALLOYING

Alloying in nanowire quantum dots seems to be inherent to the VLS growth process [3,4] and has to be addressed in any realistic modeling [18]. Importantly, the amount of phosphorous atoms due to intermixing can reach up [9,67] to 80% (i.e., leading to a $InAs_{0.2}P_{0.8}$ quantum dot) strongly affecting excitonic emission energies as well as inducing non-negligible bright exciton splitting [18] due to reduction of symmetry for C_{3v} to C_1 [15]. It is thus important to verify how alloying affects binding energies of main excitonic complexes.

[4]Single-exciton *s*-shell recombination line energy is used as a reference here since this energy was used a reference level throughout the entire paper. Notably, however, the triexciton *s*-shell recombination has energies very similar to single exciton *s*-shell recombination.

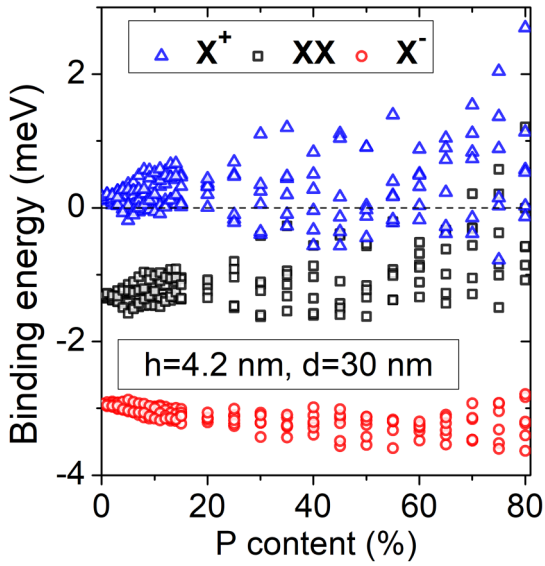

FIG. 12. Excitonic complexes' binding energies calculated as function of phosphorous content (see text for details) for a quantum dot of height equal to 4.2 nm and diameter equal to 30 nm. Colors mark different excitonic complexes. Dashed line marks zero binding energy value as a reference.

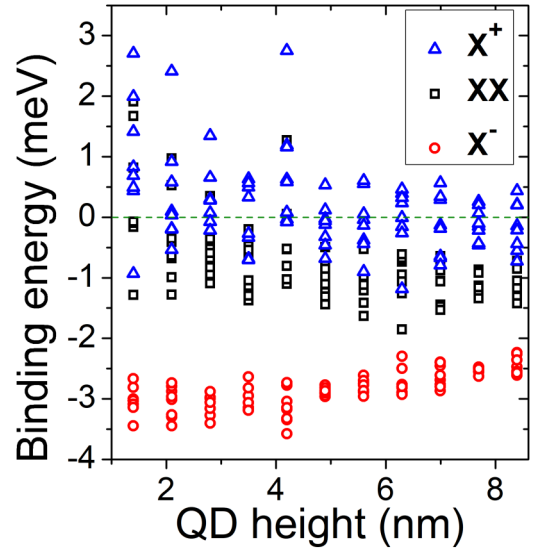

FIG. 13. Excitonic complexes' binding energies calculated as function of quantum dot height, and for fixed quantum dot diameter equal to 30 nm and phosphorus content equal to 80% ($InAs_{0.2}P_{0.8}$; see text for details). Colors mark different excitonic complexes.

Figure 12 shows the evolution of X^-, X^+, and XX binding energies with an increasing phosphorous content, for a $InAs_{1-x}P_x$ nanowire quantum dot of height equal to 4.2 nm and diameter equal to 30 nm. Here, there are altogether 29 different average P compositions varying from 0% to 80%. $x = 0$, thus zero P content, corresponds to nonalloyed, InAs quantum dot discussed in the earlier part of the paper. The P content changes from 10% to 80% with a 5% increment, and from 0% to 10% with a 1% increment for better accuracy. There are thus 28 various average compositions for alloyed quantum dots considered here, whereas for each average composition there are six randomly generated samples [18,63] leading to total of 168 different nanostructures (plus one nonalloyed case for P = 0).

Alloying leads to randomness-related spread of binding energies between different quantum dot samples. Whereas this effect plays a rather smaller role for the negatively charged exciton (Fig. 12), the impact of alloying is particularly pronounced for P contents larger than 40%, and for X^+ and XX. In case of these two complexes, alloying may not only change their absolute energies, but may even alter their energetic ordering. In some high-P content cases the biexciton may be even unbound, whereas X^+ binding energy can have both negative and positive values (from approximately -1 meV to 2 meV).

Since, in the earlier part of the paper we have determined the height as a key factor affecting nanowire quantum dot spectra, therefore, in Fig. 13 we study binding energies of excitonic complexes of interest, calculated as a function of quantum dot height, while keeping the diameter fixed and accounting for alloying by assuming P content equal to 80%. For each quantum dot height (and diameter) we generate 8 random samples leading altogether to total of 88 different nanostructures. Results obtained for P contents equal to 50%, 60%, and 70% as shown in the Appendix for comparison.

As shown in Fig. 13, alloy randomness is a strong effect that cannot be neglected in modeling of realistic intermixed quantum dots. Alloying apparently smears out some of the subtle trends discussed earlier, yet one can note that generally the order of excitonic binding energies (from lowest to highest: X^-, XX, X^+) is a typical feature of considered nanowire quantum dots. However, for highly alloyed quantum dots XX and X^+ can swap their order, especially for smaller height quantum dots. Yet (on average) the biexciton is typically weakly bound (with approximately -1 meV binding energy), whereas the positively charged trion is weakly unbound. Negatively charged exciton is again less prone to both alloying and height with binding energy values close to -3 meV. Moreover, apparently binding energy variations due to alloying seem to be more important than the role of the diameter. Additionally, alloying somewhat flattens trends related to the height dependence studied earlier.

Our results indicate that should one search for a system with small XX binding energy (e.g., crucial in certain entanglement generation schemes [68]), one should opt for highly alloyed nanowire quantum dot, yet with relatively small heights. Nevertheless, the random distribution of excitonic complexes' spectral properties demands "cherrypicking" of samples of desired properties from an ensemble of quantum dots of nominally the same sizes and average composition. Our result also indicates that the correlating results of theoretical modeling with single quantum dot experiment [69] may be significantly affected by alloying.

X. CONCLUSIONS

In this work we have studied the role of height, diameter, and alloy randomness on the main excitonic complexes' binding energies in InAs/InP nanowire quantum dots.

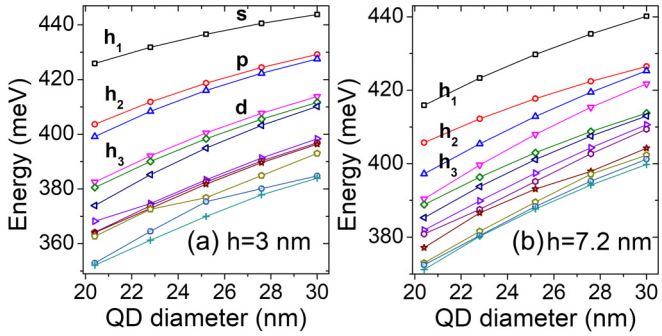

FIG. 14. Several lowest single-particle hole levels for nanowire quantum dot of (a) $h = 3$ nm and (b) $h = 7$ nm, and as a function of quantum dot diameter. Lines connect and order states energetically. h_1 is the hole ground state. s, p, and d denote approximate shells. See text for more details.

Binding energies reveal nontrivial trends with quantum dot sizes especially for larger quantum dot height and for complexes involving two hole states (the biexciton and the positively charged trion). The order of excitonic states was generally established to be X^-, XX and X^+, with rather strongly bound X^-, relatively weakly bound XX, and typically unbound X^+. We have found that trends of excitonic complexes' binding energies can be understood by means of different confinement of single-particle electron and hole states constituting these complexes, whereas piezoelectricity was determined to play a rather lesser role with a notable impact only for highest considered quantum dots. Additionally, we have studied triexciton spectra as well and obtained good qualitative agreement with the experiment, and confirmed experimental finding of $3X$ s-p shell splitting decreasing with nanowire quantum dot diameter. Next, aiming for accurate modeling of realistic nanowire quantum dots, we have presented results obtained for a family of alloyed $InAs_{1-x}P_x$. Alloying was determined to be one of the key factors affecting main complexes' binding energies, especially for phosphorus contents larger than 50%. Whereas alloying leaves X^- to be well bound, it can strongly affect XX and X^+ binding energies leading to unbound biexciton, and even reorder of binding energies XX and X^+ states.

Finally, our results indicate that apart from the control of quantum dot lateral and vertical dimensions, the control of average composition (due to related alloying) is likely necessary for tailoring of excitonic complexes' spectra in nanowire quantum dots in order to match their desired properties, and this may be essential for further nanowire quantum dot applications.

ACKNOWLEDGMENTS

M.Z. acknowledges the support from the Polish National Science Centre based on Decision No. 2018/31/B/ST3/01415.

APPENDIX A: HOLE STATES AS FUNCTION OF DIAMETER

Figure 14 shows several lowest hole levels as a function of quantum dot diameter, and for two selected quantum dot heights. For "flat" quantum dot of $h = 3$ nm the hole shell structure is present for all considered diameters, as one can unambiguously distinguish shells up to (approximately) a d shell. However, for the larger quantum dot height equal to 7.2 nm there is no apparent no-shell structure for all studied diameters. See the main text for more details.

APPENDIX B: COULOMB DIRECT INTERACTIONS J FOR GROUND ELECTRON AND HOLE STATES

Coulomb integrals J_{ee}, J_{eh}, and J_{hh} combined with Eqs. (3), (4), and (5) allow for useful estimate of exciton binding energy trends as discussed in the main part of the paper. Figure 15 shows each of these integrals separately as a function of quantum dot height and diameter. Larger-diameter quantum dots generally correspond to larger spatial single-particle states delocalization and thus smaller Coulomb interactions, which in all cases monotonically decrease with diameter. For the same reason, all these integrals generally decrease with height, with the exception of integrals involving the electron (J_{ee} and J_{eh}) and smallest considered quantum dot height ($h < 3$ nm), where the trend is reversed. Moreover, as the hole is more confined than the electron, integrals involving the hole (J_{eh} and J_{hh}) generally have larger magnitudes than electron-only terms (J_{ee}).

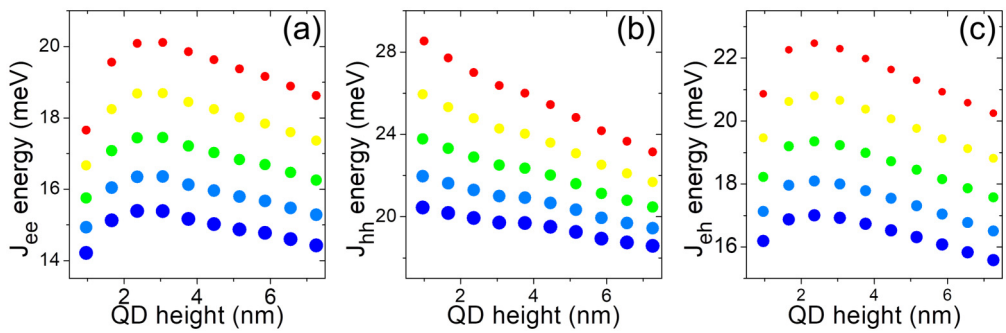

FIG. 15. Coulomb direct (a) electron-electron J_{ee}, (b) electron-hole J_{eh}, and (c) hole-hole J_{hh} integrals as a function of nanowire quantum dot and diameter. Quantum dot diameters correspond to size/color of each circle on the plot. Integrals are calculated for electron and hole in their ground states. See text for more details.

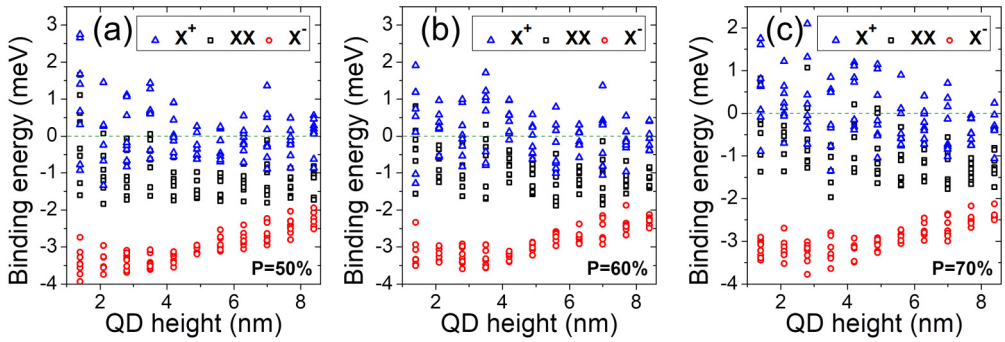

FIG. 16. Excitonic complexes' binding energies calculated as function of quantum dot height, and for fixed quantum dot diameter equal to 30 nm and phosphorus content equal to (a) 50%, (b) 60%, and (c) 70%. Colors mark different excitonic complexes.

APPENDIX C: BINDING ENERGIES FOR DIFFERENT P CONTENTS

Here, for completeness we present results of excitonic complexes' binding energy spectra, calculated as a function of quantum dot height, and for a fixed quantum dot diameter equal to 30 nm. These spectra were calculated in a way identical to those of Fig. 16, yet for three different average P contents equal to 50%, 60%, and 70%. All the pictures are qualitatively quite similar underlying the key important role of alloy randomness in modeling of nanowire quantum dot. Additionally, as shown in Fig. 16 with the increasing average P content X^+ and XX are more likely to reverse their order together with simultaneous (on average) reduction of the binding energies as discussed in the main part of the paper.

[1] B. M. T., C. Thelander, A. Hansen, L. Jensen, M. Larsson, L. R. Wallenberg, and L. Samuelson, Few-electron quantum dots in nanowires, Nano Lett. **4**, 1621 (2004).

[2] M. T. Borgström, V. Zwiller, E. Müller, and A. Imamoglu, Optically bright quantum dots in single nanowires, Nano Lett. **5**, 1439 (2005).

[3] R. S. Wagner and W. C. Ellis, Vapor-liquid-solid mechanism of single crystal growth, Appl. Phys. Lett. **4**, 89 (1964).

[4] L. E. Jensen, M. T. Björk, S. Jeppesen, A. I. Persson, B. J. Ohlsson, and L. Samuelson, Role of surface diffusion in chemical beam epitaxy of inas nanowires, Nano Lett. **4**, 1961 (2004).

[5] D. Dalacu, A. Kam, D. G. Austing, X. Wu, J. Lapointe, G. C. Aers, and P. J. Poole, Selective-area vapour–liquid–solid growth of inp nanowires, Nanotechnology **20**, 395602 (2009).

[6] Y. Chen, I. E. Zadeh, K. D. Jöns, A. Fognini, M. E. Reimer, J. Zhang, D. Dalacu, P. J. Poole, F. Ding, V. Zwiller *et al.*, Controlling the exciton energy of a nanowire quantum dot by strain fields, Appl. Phys. Lett. **108**, 182103 (2016).

[7] A. Fiset-Cyr, D. Dalacu, S. Haffouz, P. J. Poole, J. Lapointe, G. C. Aers, and R. L. Williams, In-situ tuning of individual position-controlled nanowire quantum dots via laser-induced intermixing, Appl. Phys. Lett. **113**, 053105 (2018).

[8] S. Yanase, H. Sasakura, S. Hara, and J. Motohisa, Single-photon emission from inasp quantum dots embedded in density-controlled inp nanowires, Jpn. J. Appl. Phys. **56**, 04CP04 (2017).

[9] M. Bouwes Bavinck, M. Zieliński, B. J. Witek, T. Zehender, E. P. A. M. Bakkers, and V. Zwiller, Controlling a nanowire quantum dot band gap using a straining dielectric envelope, Nano Lett. **12**, 6206 (2012).

[10] D. Dalacu, K. Mnaymneh, J. Lapointe, X. Wu, P. J. Poole, G. Bulgarini, V. Zwiller, and M. E. Reimer, Ultraclean emission from inasp quantum dots in defect-free wurtzite inp nanowires, Nano Lett. **12**, 5919 (2012).

[11] M. E. Reimer, G. Bulgarini, N. Akopian, M. Hocevar, M. B. Bavinck, M. A. Verheijen, E. P. A. M. Bakkers, L. P. Kouwenhoven, and V. Zwiller, Bright single-photon sources in bottom-up tailored nanowires, Nat. Commun. **3**, 737 (2012).

[12] S. Haffouz, K. D. Zeuner, D. Dalacu, P. J. Poole, J. Lapointe, D. Poitras, K. Mnaymneh, X. Wu, M. Couillard, M. Korkusinski *et al.*, Bright single inasp quantum dots at telecom wavelengths in position-controlled inp nanowires: the role of the photonic waveguide, Nano Lett. **18**, 3047 (2018).

[13] R. Singh and G. Bester, Nanowire Quantum Dots as an Ideal Source of Entangled Photon Pairs, Phys. Rev. Lett. **103**, 063601 (2009).

[14] M. A. Dupertuis, K. F. Karlsson, D. Y. Oberli, E. Pelucchi, A. Rudra, P. O. Holtz, and E. Kapon, Symmetries and the Polarized Optical Spectra of Exciton Complexes in Quantum Dots, Phys. Rev. Lett. **107**, 127403 (2011).

[15] K. F. Karlsson, M. A. Dupertuis, D. Y. Oberli, E. Pelucchi, A. Rudra, P. O. Holtz, and E. Kapon, Fine structure of exciton complexes in high-symmetry quantum dots: Effects of symmetry breaking and symmetry elevation, Phys. Rev. B **81**, 161307(R) (2010).

[16] M. Zieliński, Fine structure of light-hole excitons in nanowire quantum dots, Phys. Rev. B **88**, 115424 (2013).

[17] M. Świderski and M. Zieliński, Atomistic theory of excitonic fine structure in inas/inp nanowire quantum dot molecules, Phys. Rev. B **95**, 125407 (2017).

[18] M. Zieliński, Spectra of dark and bright excitons in alloyed nanowire quantum dots, Phys. Rev. B **100**, 045309 (2019).

[19] M. Zieliński, Influence of substrate orientation on exciton fine structure splitting of inas/inp nanowire quantum dots, Nanoscale Res. Lett. **7**, 265 (2012).

[20] M. Bayer, G. Ortner, O. Stern, A. Kuther, A. A. Gorbunov, A. Forchel, P. Hawrylak, S. Fafard, K. Hinzer, T. L. Reinecke, S. N. Walck, J. P. Reithmaier, F. Klopf, and F. Schäfer, Fine

structure of neutral and charged excitons in self-assembled in(ga)as/(al)gaas quantum dots, Phys. Rev. B **65**, 195315 (2002).

[21] D. Gammon, E. S. Snow, B. V. Shanabrook, D. S. Katzer, and D. Park, Fine Structure Splitting in the Optical Spectra of Single Gaas Quantum Dots, Phys. Rev. Lett. **76**, 3005 (1996).

[22] O. Benson, C. Santori, M. Pelton, and Y. Yamamoto, Regulated and Entangled Photons from a Single Quantum Dot, Phys. Rev. Lett. **84**, 2513 (2000).

[23] R. M. Stevenson, R. J. Young, P. Atkinson, K. Cooper, D. A. Ritchie, and A. J. Shields, A semiconductor source of triggered entangled photon pairs, Nature (London) **439**, 179 (2006).

[24] M. A. M. Versteegh, M. E. Reimer, K. D. Jöns, D. Dalacu, P. J. Poole, A. Gulinatti, A. Giudice, and V. Zwiller, Observation of strongly entangled photon pairs from a nanowire quantum dot, Nat. Commun. **5**, 5298 (2014).

[25] T. Huber, A. Predojevic, M. Khoshnegar, D. Dalacu, P. J. Poole, H. Majedi, and G. Weihs, Polarization entangled photons from quantum dots embedded in nanowires, Nano Lett. **14**, 7107 (2014).

[26] M. Prilmüller, T. Huber, M. Müller, P. Michler, G. Weihs, and A. Predojević, Hyperentanglement of Photons Emitted by a Quantum Dot, Phys. Rev. Lett. **121**, 110503 (2018).

[27] M. Khoshnegar, T. Huber, A. Predojević, D. Dalacu, M. Prilmüller, J. Lapointe, X. Wu, P. Tamarat, B. Lounis, P. Poole *et al.*, A solid state source of photon triplets based on quantum dot molecules, Nat. Commun. **8**, 15716 (2017).

[28] M. Zeeshan, N. Sherlekar, A. Ahmadi, R. L. Williams, and M. E. Reimer, Proposed Scheme to Generate Bright Entangled Photon Pairs by Application of a Quadrupole Field to a Single Quantum Dot, Phys. Rev. Lett. **122**, 227401 (2019).

[29] P. N. Keating, Effect of invariance requirements on the elastic strain energy of crystals with application to the diamond structure, Phys. Rev. **145**, 637 (1966).

[30] R. M. Martin, Elastic properties of zns structure semiconductors, Phys. Rev. B **1**, 4005 (1970).

[31] W. Jaskólski, M. Zieliński, G. W. Bryant, and J. Aizpurua, Strain effects on the electronic structure of strongly coupled self-assembled inas/gaas quantum dots: Tight-binding approach, Phys. Rev. B **74**, 195339 (2006).

[32] M. Zieliński, Multi-scale simulations of semiconductor nanostructures, Acta Phys. Pol. A **122**, 312 (2012).

[33] C. Pryor, J. Kim, L. W. Wang, A. J. Williamson, and A. Zunger, Comparison of two methods for describing the strain profiles in quantum dots, J. Appl. Phys. **83**, 2548 (1998).

[34] T. Saito and Y. Arakawa, Electronic structure of piezoelectric in $_{0.2}$ga $_{0.8}$n quantum dots in gan calculated using a tight-binding method, Phys. E (Amsterdam) **15**, 169 (2002).

[35] M. Zieliński, M. Korkusinski, and P. Hawrylak, Atomistic tight-binding theory of multiexciton complexes in a self-assembled inas quantum dot, Phys. Rev. B **81**, 085301 (2010).

[36] M. Zieliński, Including strain in atomistic tight-binding hamiltonians: An application to self-assembled inas/gaas and inas/inp quantum dots, Phys. Rev. B **86**, 115424 (2012).

[37] M. Zieliński, Valence band offset, strain and shape effects on confined states in self-assembled inas/inp and inas/gaas quantum dots, J. Phys.: Condens. Matter **25**, 465301 (2013).

[38] G. Bester, X. Wu, D. Vanderbilt, and A. Zunger, Importance of Second-Order Piezoelectric Effects in Zinc-Blende Semiconductors, Phys. Rev. Lett. **96**, 187602 (2006).

[39] G. Bester, A. Zunger, X. Wu, and D. Vanderbilt, Effects of linear and nonlinear piezoelectricity on the electronic properties of inas/gaas quantum dots, Phys. Rev. B **74**, 081305(R) (2006).

[40] A. Beya-Wakata, P.-Y. Prodhomme, and G. Bester, First- and second-order piezoelectricity in iii-v semiconductors, Phys. Rev. B **84**, 195207 (2011).

[41] G. Tse, J. Pal, U. Monteverde, R. Garg, V. Haxha, M. Migliorato, and S. Tomić, Non-linear piezoelectricity in zinc blende gaas and inas semiconductors, J. Appl. Phys. **114**, 073515 (2013).

[42] M. A. Caro, S. Schulz, and E. P. O'Reilly, Origin of nonlinear piezoelectricity in iii-v semiconductors: Internal strain and bond ionicity from hybrid-functional density functional theory, Phys. Rev. B **91**, 075203 (2015).

[43] D. J. Chadi, Spin-orbit splitting in crystalline and compositionally disordered semiconductors, Phys. Rev. B **16**, 790 (1977).

[44] J.-M. Jancu, R. Scholz, F. Beltram, and F. Bassani, Empirical spds* tight-binding calculation for cubic semiconductors: General method and material parameters, Phys. Rev. B **57**, 6493 (1998).

[45] S. Lee, F. Oyafuso, P. von Allmen, and G. Klimeck, Boundary conditions for the electronic structure of finite-extent embedded semiconductor nanostructures, Phys. Rev. B **69**, 045316 (2004).

[46] *Topics in Applied Physics*, Vol. 90, edited by P. Michler (Springer, New York, 2003).

[47] G. Onida, L. Reining, and A. Rubio, Electronic excitations: density-functional versus many-body green's-function approaches, Rev. Mod. Phys. **74**, 601 (2002).

[48] M. Cygorek, M. Korkusinski, and P. Hawrylak, Atomistic theory of electronic and optical properties of inasp/inp nanowire quantum dots, Phys. Rev. B **101**, 075307 (2020).

[49] Y.-M. Niquet and D. C. Mojica, Quantum dots and tunnel barriers in in as/ in p nanowire heterostructures: Electronic and optical properties, Phys. Rev. B **77**, 115316 (2008).

[50] A. J. Williamson, L. W. Wang, and A. Zunger, Theoretical interpretation of the experimental electronic structure of lens-shaped self-assembled inas/gaas quantum dots, Phys. Rev. B **62**, 12963 (2000).

[51] A. Franceschetti and A. Zunger, Pseudopotential calculations of electron and hole addition spectra of inas, inp, and si quantum dots, Phys. Rev. B **62**, 2614 (2000).

[52] E. Burstein and A. Pinczuk, *The Physics of Opto-electronic Materials* (Plenum, New York, 1971), p. 33.

[53] M. Levinshtein, *Handbook Series on Semiconductor Parameters*, Vol. 1 (World Scientific, Singapore, 1997).

[54] Y. M. Niquet, Electronic and optical properties of in as/ ga as nanowire superlattices, Phys. Rev. B **74**, 155304 (2006).

[55] S. Lee, L. Jönsson, J. W. Wilkins, G. W. Bryant, and G. Klimeck, Electron-hole correlations in semiconductor quantum dots with tight-binding wave functions, Phys. Rev. B **63**, 195318 (2001).

[56] S. Schulz, S. Schumacher, and G. Czycholl, Tight-binding model for semiconductor quantum dots with a wurtzite crystal structure: From one-particle properties to coulomb correlations and optical spectra, Phys. Rev. B **73**, 245327 (2006).

[57] P. T. Różański and M. Zieliński, Linear scaling approach for atomistic calculation of excitonic properties of 10-million-atom nanostructures, Phys. Rev. B **94**, 045440 (2016).

[58] P. T. Różański and M. Zieliński, Efficient computation of coulomb and exchange integrals for multi-million atom nanostructures, Comput. Phys. Commun. **238**, 254 (2019).

[59] D. Bimberg, M. Grundmann, and N. Ledentsov, *Quantum Dot Heterostructures* (Wiley, Chichester, 1999).

[60] L. Jacak, P. Hawrylak, and A. Wojs, *Quantum Dots* (Springer, Berlin, 1998).

[61] M. Gong, K. Duan, C.-F. Li, R. Magri, G. A. Narvaez, and L. He, Electronic structure of self-assembled inas/inp quantum dots: Comparison with self-assembled inas/gaas quantum dots, Phys. Rev. B **77**, 045326 (2008).

[62] M. Zieliński, From quantum dots to quantum dashes: Excitonic spectra of highly elongated inas/inp nanostructures, Phys. Rev. B **99**, 205402 (2019).

[63] M. Zieliński, K. Gołasa, M. R. Molas, M. Goryca, T. Kazimierczuk, T. Smoleński, A. Golnik, P. Kossacki, A. A. L. Nicolet, M. Potemski, Z. R. Wasilewski, and A. Babiński, Excitonic complexes in natural inas/gaas quantum dots, Phys. Rev. B **91**, 085303 (2015).

[64] M. Grundmann, *Physics of Semiconductors*, Vol. 11 (Springer, Berlin, 2010).

[65] A. Schliwa, M. Winkelnkemper, A. Lochmann, E. Stock, and D. Bimberg, In(ga)as/gaas quantum dots grown on a (111) surface as ideal sources of entangled photon pairs, Phys. Rev. B **80**, 161307(R) (2009).

[66] O. Stier, M. Grundmann, and D. Bimberg, Electronic and optical properties of strained quantum dots modeled by 8-band k·p theory, Phys. Rev. B **59**, 5688 (1999).

[67] M. van Weert, Quantum Dots in Vertical Nanowire Devices, Ph.D. thesis (Technische Universiteit Delft, The Netherlands, 2011).

[68] M. Khoshnegar and A. H. Majedi, Entangled photon pair generation in hybrid superconductor–semiconductor quantum dot devices, Phys. Rev. B **84**, 104504 (2011).

[69] V. Mlinar, M. Bozkurt, J. M. Ulloa, M. Ediger, G. Bester, A. Badolato, P. M. Koenraad, R. J. Warburton, and A. Zunger, Structure of quantum dots as seen by excitonic spectroscopy versus structural characterization: Using theory to close the loop, Phys. Rev. B **80**, 165425 (2009).